G-band Variation of Individual Single-Walled Carbon Nanotubes under Torsional Strain

Bo Gao,[†] Xiaojie Duan,[†] Jin Zhang,*[,†] Gang Wu,[‡] Jinming Dong,[‡] and Zhongfan Liu*[,†]

Centre for Nanoscale Science and Technology (CNST), Beijing National Laboratory for Molecular Sciences (BNLMS), Key Laboratory for the Physics and Chemistry of Nanodevices, State Key Laboratory for Structural Chemistry of Unstable and Stable Species, College of Chemistry and Molecular Engineering, Peking University, Beijing 100871, People's Republic of China, and Group of Computational Condensed Matter Physics, National Laboratory of Solid State Microstructures and Department of Physics, Nanjing University, Nanjing 210093, People's Republic of China

Received: April 21, 2008; Revised Manuscript Received: April 28, 2008

Strain can effectively modulate the structure and properties of single-walled carbon nanotubes (SWNTs), and hence is an important aspect in their researches and applications. In this article, the effect of torsional strain on the *G*-band modes of individual SWNTs is reported. When torsional strain is induced by atomic force microscopy (AFM) manipulation, *G*-band of SWNTs varies significantly. Following *G*-band modes ($2A_{1g}$, $2E_{1g}$, and $2E_{2g}$) assignment by polarized resonant Raman spectroscopy, it is found that modes with different symmetries respond quite differently to torsional strain. On the basis of the analyses of eight individual SWNTs, we find that the variation of *G*-band is sensitive to the diameter and chirality of SWNTs. Finally, the nonresonant Raman spectra of chiral (12, 4) SWNTs are calculated using the *ab initio* calculations and the empirical bond polarizability model, which further confirms that there are some relations between mode symmetries and the effect of torsional strain on Raman spectra.

I. Introduction

Single-walled carbon nanotubes (SWNTs) are molecular-scale tubes of graphitic carbon with outstanding properties, which are obtained by wrapping a graphene sheet into a seamless cylinder usually with diameters of 1−2 nm. Their unique 1D structure and diverse chiral index endow SWNTs with different electronic structure and phonon property, further giving rise to characteristic Raman spectra.

Raman spectroscopy is an important aspect in the research of SWNTs and is also a powerful tool in characterizing SWNTs, including electronic structure, physical and mechanical properties.[1] The observation of Raman spectra from just one individual SWNT[2] is an important breakthrough, which makes it possible to investigate the geometry structure, electronic structure, and physical properties of individual SWNTs with specified chiral index. There are two important first-order features in Raman spectra of SWNTs: the radial breathing mode (RBM) with A_{1g} symmetry and the tangential *G*-band composed of six modes: A_{1g}^+ and A_{1g}^-, E_{1g}^+ and E_{1g}^-, E_{2g}^+ and E_{2g}^-. The RBM where all atoms vibrate in phase in the radial direction is the characteristic phonon mode of SWNTs and can be used to estimate chiral indices (n, m)[2,3] and electronic transition energy E_{ii}.[4] Very recently, the RBM has been found to be an indication of the torsional strain in SWNTs.[5] The *G*-band, which comes from the graphite tangential $E_{2g}(2)$ Raman active mode, can be used to characterize the diameter,[6] to perform polarization analysis of Raman spectra,[7,8] and to probe uniaxial strain in SWNTs.[5,9] Therefore, Raman spectra of individual SWNTs facilitate us to investigate the relationship between strain-induced geometry structure transformation and vibrational properties of individual SWNTs.

Various methods[5,9–14] have been used to introduce strains into individual SWNTs and their Raman spectra under strains have been studied theoretically[15,16] and experimentally.[5,9,10,12,13] Hydrostatic pressure[10] and atomic force microscopy (AFM) tip indentation[11,12] are widely used to induce radial compression. By first principle calculations, Dong et al. systematically investigated structural property and Raman spectra of SWNTs under hydrostatic pressure and found an upshift of RBM which could distinguish three different collapsed structures of SWNTs under hydrostatic pressure.[15] Lebedkin et al. experimentally studied the hydrostatic pressure dependence of Raman spectra for different SWNTs and observed reversible upshift of Raman spectra in the low pressure regime.[10] But in the high pressure regime, disappearance of RBMs and *G*-bands, increase of defects-induced *D*-bands, and other irreversible effects in Raman spectra occurred. Yano et al. investigated nanoscale pressure effect of AFM tip on isolated SWNT bundles by using tip-enhanced near-field Raman spectroscopy (TERS)[12] and found frequency of G^- downshifted as much as 18 cm^{-1}, whereas frequency of G^+ did not shift with increasing the AFM-tip force. Theoretical models show significant variation of Raman spectra under uniaxial strain and torsional strain. By *ab initio* calculations, Dong et al. found that under uniaxial strain *G*-band of Raman spectra shifted downward linearly for any kind of SWNTs due to bond elongation, while under torsional strain some modes of *G*-band were downshifted and some upshifted, which was because some bonds elongated and some shortened.[16] Evidence for these variations under uniaxial strain have been observed experimentally by stretching SWNTs in composites[13] or by atomic force microscopy (AFM) tip manipulation.[5,9] Young et al. collected the Raman spectra of nanotube composite materials (such as nanotubes in epoxy) under uniaxial strain (both tension and compression) and found the downshift of G'-band (∼2700 cm^{-1}) was proportional to uniaxial strain.[13] Cronin et al. stretched individual SWNTs by AFM tip and studied the

* To whom correspondence should be addressed. (J.Z.) Tel. and Fax: 86-10-6275-7157. Email: jinzhang@pku.edu.cn.
† Peking University.
‡ Nanjing University.

10.1021/jp803434y CCC: $40.75
Published on Web 06/26/2008

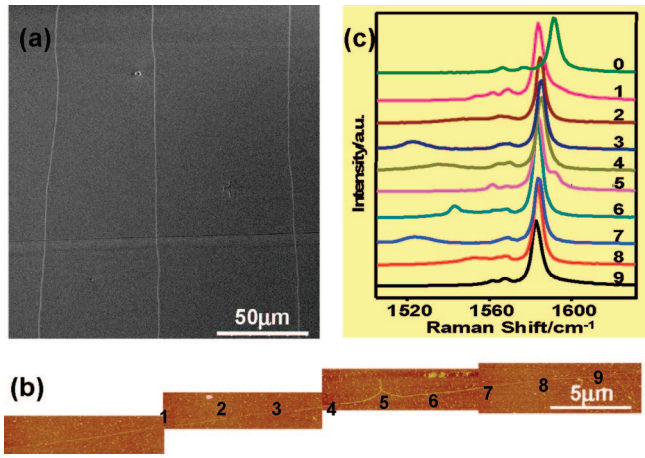

Figure 1. (a) A typical SEM image of ultralong SWNTs used for AFM manipulation. (b) A typical tapping mode AFM image of SWNTs after AFM manipulation. (c) *G*-band of (14, 2) SWNT before and after AFM manipulation. "0" is the original spectra before manipulation. "1" −"9" are the after-manipulation spectra of nine points along SWNTs indicated in panel b.

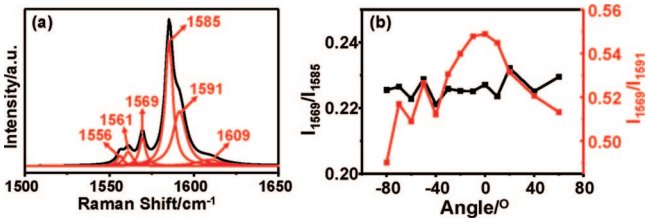

Figure 2. (a) Lorentzian fits to the *G*-band of (13, 11) SWNT. Black lines are original data and red lines are fitted peaks. The peak positions are labeled by red number. (b) Intensity ratio between 1569 and 1585 cm^{-1} (black) and between 1569 and 1591 cm^{-1} (red) as a function of the angle. The angle is between the SWNTs axis and the incident-light polarization.

effects of uniaxial strain on Raman spectra and electronic structures.[17] They found the downshifts of *G*-band induced by uniaxial strain did not scale proportionally for different SWNTs and appeared to be quite sensitive to chirality. However, the torsional strain effects on Raman spectra and other properties of SWNTs are less studied experimentally. This is probably because torsional strain is difficult to prepare and "see". Meyer et al. built a torsional pendulum based on SWNTs by nanolithography.[14] By electrically rotating the metal block, quantitative elastic torsional strain was resulted. Recently, using AFM manipulation, torsional and uniaxial strains have been introduced in individual SWNTs.[5] It is found that the RBM and *G*-band spectra respond differently to the two types of strains. Under uniaxial strain, the RBM frequency (ω_{RBM}) and the highest frequency mode in the *G*-band, which occurs around ~1600 cm^{-1}, do not have a noticeable response; in contrast, the other observed modes of the *G*-band are downshifted. Under torsional strain, ω_{RBM} is found to upshift, and the *G*-band is found to split into multiple sub-bands in some cases, presumably due to the broken symmetry induced by torsion. The highest frequency mode in the *G*-band downshifts significantly under torsional strain, whereas the other observed modes of the *G*-band slightly upshift. However, the effect of torsional strain on different modes of the *G*-band has not been investigated in detail.

In this work, the effect of torsional strain on each mode of the *G*-band of individual SWNTs was reported. When torsional strain is induced by AFM manipulation, *G*-band of SWNTs varies significantly. Following *G*-band modes ($2A_{1g}$, $2E_{1g}$, and $2E_{2g}$) assignment by polarized resonant Raman spectroscopy, it is found that modes with different symmetries respond quite differently to torsional strain. On the basis of the analyses of eight individual SWNTs, we find that the variation of *G*-band is sensitive to the diameter and chirality of SWNTs and the quasiacoustic plasmon mode in SWNTs. Finally, the nonresonant Raman spectra of chiral (12, 4) SWNTs are calculated using the *ab initio* calculations and the empirical bond polarizability model, which further confirms that there are some relations between mode symmetries and the effect of torsional strain on Raman spectra. The details and understandings of these variations will be discussed in this paper.

II. Experiment

As shown in Figure 1a, SWNTs were grown on silicon substrate with a 1 μm thick oxide layer from ethanol chemical vapor deposition and had a typical length of several millimeters.[18] The substrates, which were fabricated by photolithography, have trenches and crosses as markers which are used to position SWNTs for AFM manipulation and Raman spectral characterization. High orientation and straightness of ultralong SWNTs could eliminate the effect of laser polarization on frequency and intensity of Raman spectra. The AFM manipulation was conducted by using Nanoscope III SPM (Veeco) with specifically compiled software. Normally the AFM was operated in tapping mode AFM in air. For a typical manipulation, AFM tip was pressed down about 50 nm with feedback switched off. After that, the tip moved horizontally at the speed of 0.5 μm/s along a predefined path perpendicular to the tube axis. Then the tip returned to normal imaging distance, and the feedback was switched on to get images of manipulated SWNTs. During manipulation, SWNT would roll on substrate due to the friction between them. It can be seen that the SWNT has been dragged away from the manipulation point (Figure 1b), revealing that frictional forces between the tube and the substrate are strong enough to maintain the strain in SWNT after the removal of AFM tip, which provides an opportunity to perform ex-situ characterization of the strain in SWNT.

Raman spectral characterization was performed before and after manipulation by using Renishaw 1000 micro-Raman spectroscopy (~1 μm spot size) with a 632.8 nm (1.959 eV) He−Ne laser with laser power of 8 mW. The gratings were kept in the extended option. By aligning the laser spot relative to the markers, we can ensure that laser polarization direction is parallel to SWNT axis and Raman spectra at a specific site are obtained. Before manipulation, Raman spectra taken at different points along the axis of ultralong SWNTs are identical, indicating that ultralong SWNTs have the same diameter and chirality over millimeters of length. All the Raman spectra were fitted to Lorentzian peak shape to obtain the peak frequency, peak intensity, and full width at half-maximum (fwhm), and were calibrated by Rayleigh scattering. Chiral indices (n, m) were assigned based on the characteristic frequency, peak intensity, and fwhm.[19]

In order to elucidate the variation of *G*-band under torsional strain, polarized resonant Raman spectroscopy was performed to assign *G*-band modes. According to symmetry selection rules for the first-order single-resonance Raman scattering process,[6,7] six modes ($2A_{1g}$, $2E_{1g}$ and $2E_{2g}$) can be observed. To perform the polarized Raman experiment, a $\lambda/2$ plate was placed close to the sample to rotate both the incident and backscattered light. A fixed polarizer was placed close to the charge-coupled device (CCD) detector to analyze scattered light polarized parallel to the incident-light polarization (VV configuration). By rotating

TABLE 1: Modes Assignment of *G*-band Raman Spectra from Eight Individual SWNTs Based on Symmetry Selection Rules for the First-Order Single-Resonance Raman Scattering Process[a]

RBM (cm^{-1})	(n, m)	E_{2g}^+ (cm^{-1})	A_{1g}^+ (cm^{-1})	E_{1g}^+ (cm^{-1})	E_{1g}^- (cm −1)	A_{1g}^- (cm^{-1})	E_{2g}^- (cm^{-1})	BWF (cm^{-1})
141.4	(15, 10)	1601.5	1589.8	x	1578.8	1565.3	x	x
148.5	(13, 11)	1609.3	1585.3	1591.4	1561.4	1569.0	1556.1	x
155.9	(16, 6)	1599.5	1581.6	1580.3	1575.3	1565.2	1555.6	x
160.6	(12, 10)	1604.2	1585.8	1584.2	1568.9	1564.0	x	x
198.9	(14, 2)	1600.8	1583.7	x	x	1560.0	x	1541.1
211.9	(11, 5)	1593.5	1588.7	x	x	x	x	x
218.6	(12, 3)	1592.1	1585.7	x	x	x	x	x
285.8	(7, 5)	1596.5	1582.0	x	x	1536.6	x	x

[a] All the RBM were collected before manipulation and calibrated by Rayleigh scattering. Chiral indices (n, m) are assigned based on frequencies and intensities. "x" means the modes were not observed.

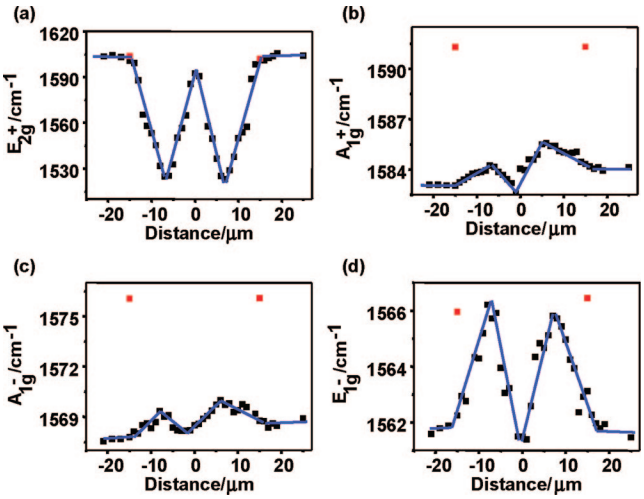

Figure 3. Frequency profiles of (a) E_{2g}^+, (b) A_{1g}^+, (c) A_{1g}^-, and (d) E_{1g}^- modes along (13, 11) SWNT axis after manipulation. Red squares and black squares are frequencies before and after manipulation respectively. Black lines are linear curve-fitted results. The manipulation point is at 0 μm.

the $\lambda/2$ plate, G-band with different φ (the angle between the SWNTs axis and the incident-light polarization) was obtained.

III. Results and Discussions

A. Torsional Strain Effect on *G*-band. An individual SWNT with ω_{RBM} at 148.5 cm^{-1}, assigned as (13, 11)[19] with a calculated diameter of 1.65 nm and chiral angle of 27.2°, was manipulated. Before manipulation, tapping mode AFM measurement gave a diameter of 1.4 nm which indicates the tube is not a bundle or multiwalled carbon nanotube (MWNT). The original *G*-band spectra close to the manipulation point is shown in Figure 1c and is labeled by "0". After manipulation, the SWNT was dragged away the manipulation point by about 0.767 μm. The *G*-band spectra at nine points (indicated in Figure 1b) along the tube axis are shown in Figure 1c and are labeled by "1"−"9", where point "5" is the manipulation point. It can be seen that the *G*-band spectra vary significantly along SWNTs, which reveals a mixing effect of both uniaxial and torsional strain:[5] uniaxial strain makes all the peaks downshift except the peak at the highest frequency; while torsional strain makes the peak at the highest frequency downshift remarkably, but other peaks upshift a little. It is noteworthy that in the torsional region *G*-band spectra at nine points vary gradually and immonotonously along the tube axis. This indicates torsional strain is not uniformly distributed, but shows a gradual variation, in "M" shape along the tube axis, which is due to the balance of torsinal strain in SWNTs and frictional forces by substrate. Under the AFM manipulation the strain decreases along the tube axis starting from the manipulation point because of the substrate friction that acts on the movement of the SWNTs. If the friction at each point is constant, the decrease will be linear, resulting in "Λ" shape distribution of torsional strain. After the tip is removed, the elastic retraction of the nanotubes in combination with the friction will result in "M" shape distribution along the tube axis. Similar phenomena are also observed from other seven SWNTs.

B. *G*-band Modes Assignment. Figure 2a shows the VV *G*-band spectra of the (13, 11) SWNT. The angle φ between the SWNTs axis and the incident-light polarization is 80°. The spectra can be fit by six well-defined Lorentzian peaks. From previous polarization Raman studies,[7] the peaks at 1609 and 1556 cm^{-1} should be assigned as E_{2g}^+ and E_{2g}^- modes, respectively. Due to the larger intensity of A_{1g} symmetry mode,[7] the peaks at 1585 and 1591 cm^{-1} are assigned as A_{1g}^+ and E_{1g}^+ modes respectively. The dependence of the intensity ratio between 1569 and 1585 cm^{-1} (I_{1569}/I_{1585}) and between 1569 and 1591 cm^{-1} (I_{1569}/I_{1591}) on the angle φ is shown in Figure 2b. It can be seen that the ratio I_{1569}/I_{1585} does not almost vary and is independent of the angle φ, while the ratio I_{1569}/I_{1591} depends on the incident light polarization direction. So the peak at 1569 cm^{-1} should have the same mode symmetry as that at 1585 cm^{-1} and is assigned as A_{1g}^- mode. The peak at 1561 cm^{-1} is assigned as E_{1g}^- mode. Modes assignment of *G*-band Raman spectra from other seven individual SWNTs were also performed based on symmetry selection rules for the first-order single-resonance Raman scattering process (shown in Table 1).

C. Torsional Strain Effect on *G*-band Modes. Effects of strains on *G*-band modes of individual (13, 11) SWNT were shown in Figure 3, where we mapped the ultralong SWNT and plotted the frequencies of E_{2g}^+, A_{1g}^+, A_{1g}^-, and E_{1g}^- modes versus the distance away from the manipulation point. As the spectra are calibrated by Rayleigh scattering and the upshifts/downshits are obtained by linear curve fitting, the precision here can amount to 0.1 cm^{-1}. It can be seen from Figure 3a that uniaxial strain has no effect on E_{2g}^+ mode, but torsional strain makes E_{2g}^+ mode downshift by a maximum of about 79.0 cm^{-1} (shown in Table 2). However, as show in Figure 3b−d, uniaxial strain makes A_{1g}^+, A_{1g}^-, and E_{1g}^- modes downshift by a maximum of about 8.0, 8.0, and 4.5 cm^{-1}, but torsional strain makes them upshift by a maximum of about 1.4, 1.5, and 4.5 cm^{-1} (shown in Table 2). Due to small intensities of E_{1g}^+ and E_{2g}^- modes at most points of the SWNT, these two modes are not plotted, but we still can observe the E_{2g}^- mode downshifts under uniaxial strain and upshifts under torsional strain. Cronin et al. have observed the downshift of *G*-band under uniaxial strain, and they attributed this to the elongation of C−C bonds which weakens the bond and therefore lowers the vibrational frequency. On contrast, dependence of *G*-band on torsional strain

TABLE 2: The Maximal *G*-band Variation of Eight Manipulated Ultra-long SWNTs[a]

RBM (cm^{-1})	(n, m)	d_t(theo.) (nm)	θ (°)	Δd (μm)	E_{2g}^+ (cm^{-1})	A_{1g}^+ (cm^{-1})	E_{1g}^+ (cm^{-1})	E_{1g}^- (cm^{-1})	A_{1g}^- (cm^{-1})	E_{2g}^- (cm^{-1})	BWF (cm^{-1})
141.4	(15, 10)	1.73	23.4	1.160	−52.0	+0.5	x	+2.0	+1.0	x	x
148.5	(13, 11)	1.65	27.2	0.767	−79.0	+1.4	x	+4.5	+1.5	+	x
155.9	(16, 6)	1.54	15.3	0.484	−33.0	+1.0	+1.0	+	+0.8	+2.0	x
160.6	(12, 10)	1.51	27.0	0.775	−66.0	+1.0	+1.0	+3.6	+1.0	x	x
198.9	(14, 2)	1.20	6.59	1.142	−26.0	−27.0	x	x	−30.0	x	−51.0
211.9	(11, 5)	1.13	17.8	2.428	−91.0	+1.2	x	x	x	x	x
218.6	(12, 3)	1.09	10.9	0.658	−75.0	+1.4	x	x	x	x	x
285.8	(7, 5)	0.83	24.5	0.573	−29.0	+0.5	x	x	+0.5	x	x

[a] All the RBM were collected before manipulation and calibrated by Rayleigh scattering. Chiral indices (n, m) are assigned based on frequencies and intensities. Diameter d_t and chiral angle θ are calculated based on chiral indices (n, m). Δd is the distance away from the manipulation point. "x" means the modes were not observed.

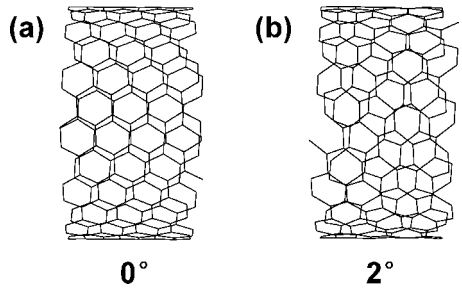

Figure 4. Geometrical structure of (13, 11) SWNT (a) without torsional strain and (b) with torsional angle 2°. Torsional-strain-induced geometrical structure transformation makes some bonds elongate and some bonds shorten.

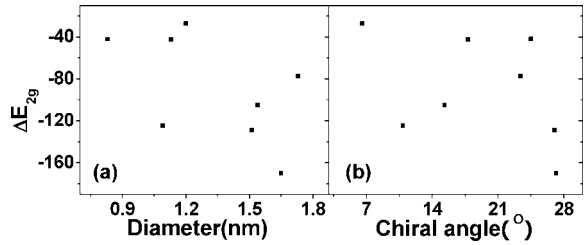

Figure 5. The relationship between the torsional strain induced downshift of E_{2g}^+ mode and (a) diameter and (b) chiral angle. For comparison, the maximal downshift of E_{2g}^+ mode was divided by the manipulation distance and then was multiplied by the diameter of SWNTs, to obtain SWNTs with the same torsional status.

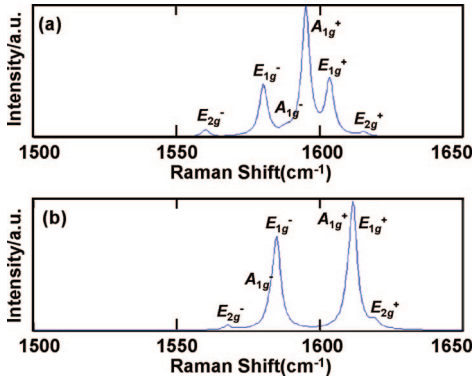

Figure 6. Calculated *G*-band spectra of (12, 4) SWNT (a) without torsional strain and (b) with torsional angle 0.89397°. The *G*-band is composed of six modes: A_{1g}^+ and A_{1g}^-, E_{1g}^+ and E_{1g}^-, E_{2g}^+ and E_{2g}^-.

is more complicated; some modes upshift and others downshift. As shown in Figure 4, torsional-strain-induced geometry structure transformation makes some bonds elongate and some bonds shorten.[16] It can also be seen from Figure 3 and Table 2, under torsional strain, the maximal variation of E_{2g}^+ mode is far larger than that of A_{1g}^+, A_{1g}^-, and E_{1g}^- modes, but there is not remarkable differences among the maximal variations of A_{1g}^+, A_{1g}^-, and E_{1g}^- modes, indicating that each mode depends on different bonds, whose force constants vary differently under torsional strain.

As listed in Table 2, we have collected and analyzed *G*-band of eight individual ultralong SWNTs, including four semiconducting tubes and four metallic tubes. Of eight individual SWNTs, *G*-band of seven individual SWNTs has similar respondence to torsional strain. E_{2g}^+ mode downshifts significantly, even by 91 cm^{-1}; A_{1g}^+, A_{1g}^-, E_{1g}^+, E_{1g}^-, and E_{2g}^- modes upshift a little, ordinarily by several wave numbers. For any one SWNT, the upshifts of A_{1g}^+, A_{1g}^-, and E_{1g}^+ modes are almost similar, and E_{1g}^- mode upshifts 3−4 times as that of A_{1g}^+, A_{1g}^-, and E_{1g}^+ modes. This indicates the effect of torsinal strain on *G*-band modes is related to mode symmetries. Hence, the response of *G*-band modes to torsional strain can be a good method of assigning *G*-band mode symmetries.

Effects of strains on SWNTs have been reported to be related to chiral index,[20–22] and particularly, uniaxial strain has been used to assign chiral index.[23] Figure 5 shows the relationship between torsional strain induced downshift of E_{2g}^+ mode and chiral index, including diameter and chiral angle respectively. SWNTs are assumed to roll on substrate without slippage. In order to compare SWNTs with the same torsional angle, we divide the maximal downshift of E_{2g}^+ mode by the manipulation distance, and then multiply by the diameter of SWNTs. As shown in Figure 5, the downshift of the E_{2g}^+ mode increase with the diameter and chiral angle increasing, indicating chiral index plays an important role in torsional strain effect on *G*-band modes. Hence, the response of *G*-band to torsional strain can be used to assign chiral index.

As shown in Table 2, *G*-band modes of (14, 2) SWNT and torsional-strain-induced variation are different from other seven SWNTs. The *G*-band has a broad and asymmetric Breit−Wigner−Fano (BWF) line shape at lower frequency, indicating the quasiacoustic plasmon mode in SWNT forms hybrid excitations with phonon mode.[24] Under torsional strain, all modes downshift to lower frequencies significantly (tens of wave numbers). It is probably the interaction between quasiacoustic plasmon mode and *G*-band modes that changed the torsional strain effect on *G*-band modes.

IV. Ab Initio Calculation

In order to elucidate the *G*-band variation of SWNTs under torsional strain, the nonresonant Raman spectra were calculated using the *ab initio* calculations and the empirical bond polarizability model.[16] The first principle calculations are based on the total energy plane-wave pseudopotential method in the local density approximation (LDA) and the Vienna *ab initio* simulation package (VASP) is employed in this paper. A supercell geometry was adopted and the K-points sampling in the

TABLE 3: Calculated Frequencies of *G*-band of (12, 4) SWNT at Torsional Angles of 0 and 0.89397°[a]

Torsional Angle (°)	E_{2g}^{+} (cm^{-1})	E_{1g}^{+} (cm^{-1})	A_{1g}^{+} (cm^{-1})	A_{1g}^{-} (cm^{-1})	E_{1g}^{-} (cm^{-1})	E_{2g}^{-} (cm^{-1})
0	1615.22	1603.54	1595.23	1588.31	1580.32	1560.13
0.89397	1619.14	1609.41	1611.47	1582.59	1584.82	1567.71
ΔG	3.92	5.87	16.24	−5.72	4.50	7.58

[a] ΔG is the frequency variation of each mode.

reciprocal space is a uniform grid ($1 \times 1 \times n$) along the tube axis. We use cumulant force constant (CFC) method to construct the dynamical matrices for SWNTs and then calculate their phonon dispersion curves, where the line shape of each peak is assumed to be Lorentzian and its line width is fixed at 1.68 cm^{-1}. The SWNTs geometric structures have been fully optimized before performing CFC calculation. In our calculations, the SWNT keeps a cylinder structure and does not show any structure transformations and defects under torsional strain. The final residual forces acting on all the atoms were less than 0.01 eV/Å. The equilibrium lattice constant along tube axis and averaged nanotube radius are 15.28 and 5.636 Å, respectively. Since all nanotubes used in our experiment are chiral ones, which are too large for our *ab initio* calculation, the chiral (12, 4) SWNT is taken as an example. The torsional angle γ is defined as done by L. Yang.[22]

The calculated *G*-band spectra of (12, 4) SWNT with and without torsional strain is shown in Figure 6, which is composed of six modes: A_{1g}^{+} and A_{1g}^{-}, E_{1g}^{+} and $E_{1\,g}^{-}$, and E_{2g}^{+} and E_{2g}^{-}. Consistent with experiment, under torsional strain, some modes of *G*-band upshift and some downshift (e.g., A_{1g}^{-} mode). It is originated from different change behavior of C−C bonds under torsional strain; some are elongated and some are shortened[16].

The calculated frequencies of *G*-band with and without torsional strain are shown in Table 3. It can be seen that, with torsional angle γ increasing from 0 to 0.89397°, E_{1g}^{+}, E_{1g}^{-}, E_{2g}^{-}, and A_{1g}^{+} modes upshift by 5.87, 4.50, 7.58, and 16.24 cm^{-1}, respectively, where the variations of the former three modes are similar, but the variation of A_{1g}^{+} mode is about 3 times as that of the former three modes. This is partly consistent with the experimental data in Table 2, which confirms our speculation that the effect of torsinal strain on *G*-band modes is dependent on mode symmetries. Comparing each variation of the above four modes theoretically (shown in Table 3) and experimentally (shown in Table 2), it is found that the maximal experimental variations are about 1/4 to 1/3 of the calculated ones. We could infer that the maximal experimental torsional angle is around 0.23°, which is small enough to be kept by interactions between substrate and SWNTs. However, the calculated variations of E_{2g}^{+} and A_{1g}^{-} modes are inconsistent with experimental results (shown in Table 2). So, more investigations are needed to reveal the intrinsic mechanism to induce the variation of *G*-band under torsional strain.

V. Summary

In summary, the work gives the first systematically experimental study of the torsional strain effect on modes of *G*-band of individual SWNTs. When torsional strain is induced by AFM manipulation, *G*-band of SWNTs varies accordingly. Following *G*-band modes assignment by polarized resonant Raman spectroscopy, it is found that modes with different symmetries respond quite differently to torsional strain. On the basis of the analyses of eight individual SWNTs, we find that the variation of *G*-band is sensitive to the tube diameter and chirality. Also the quasiacoustic plasmon mode has significant effect on the torsional strain-induced variation of *G*-band. Finally, the nonresonant Raman spectra of chiral (12, 4) SWNTs are calculated using the *ab initio* calculations and the empirical bond polarizability model, which further confirms the relations between mode symmetries and the effect of torsional strain on Raman spectra. These findings not only help us understand the origin of the *G*-band modes with different symmetries, but also endow us with the ability to characterize torsional strains in SWNTs by Raman spectra.

Acknowledgment. This work was supported by NSFC (Grants 20573002, 20673004, 20725307, and 50521201) and MOST (Grants 2006CB932701, 2006CB932403, and 2007CB936203).

References and Notes

(1) Dresselhaus, M. S.; Dresselhaus, G.; Jorio, A. *J. Phys. Chem. C* **2007**, *111*, 17887.
(2) Jorio, A.; Saito, R.; Hafner, J. H.; Lieber, C. M.; Hunter, M.; McClure, T.; Dresselhaus, G.; Dresselhaus, M. S. *Phys. Rev. Lett.* **2001**, *86*, 1118.
(3) Yu, Z.; Brus, L. E. *J. Phys. Chem. C* **2001**, *105*, 6831.
(4) Souza, A. G.; Jorio, A.; Hafner, J. H.; Lieber, C. M.; Saito, R.; Pimenta, M. A.; Dresselhaus, G.; Dresselhaus, M. S. *Phys. Rev. B* **2001**, *63*, 241404.
(5) Duan, X. J.; Son, H. B.; Gao, B.; Zhang, J.; Wu, T. J.; Samsonidze, G. G.; Dresselhaus, M. S.; Liu, Z. F.; Kong, J. *Nano Lett.* **2007**, *7*, 2116.
(6) Jorio, A.; Souza, A. G.; Dresselhaus, G.; Dresselhaus, M. S.; Swan, A. K.; Unlu, M. S.; Goldberg, B. B.; Pimenta, M. A.; Hafner, J. H.; Lieber, C. M.; Saito, R. *Phys. Rev. B* **2002**, *65*, 155412.
(7) Jorio, A.; Pimenta, M. A.; Souza, A. G.; Samsonidze, G. G.; Swan, A. K.; Unlu, M. S.; Goldberg, B. B.; Saito, R.; Dresselhaus, G.; Dresselhaus, M. S. *Phys. Rev. Lett.* **2003**, *90*, 107403.
(8) Jorio, A.; Souza, A. G.; Brar, V. W.; Swan, A. K.; Unlu, M. S.; Goldberg, B. B.; Righi, A.; Hafner, J. H.; Lieber, C. M.; Saito, R.; Dresselhaus, G.; Dresselhaus, M. S. *Phys. Rev. B* **2002**, *65*, 121402.
(9) Cronin, S. B.; Swan, A. K.; Unlu, M. S.; Goldberg, B. B.; Dresselhaus, M. S.; Tinkham, M. *Phys. Rev. Lett.* **2004**, *93*, 167401.
(10) Lebedkin, S.; Arnold, K.; Kiowski, O.; Hennrich, F.; Kappes, M. M. *Phys. Rev. B* **2006**, *73*, 94109.
(11) Wang, H. Y.; Zhao, M.; Mao, S. X. *Appl. Phys. Lett.* **2006**, *89*, 211906.
(12) Yano, T. A.; Inouye, Y.; Kawata, S. *Nano Lett.* **2006**, *6*, 1269.
(13) Cooper, C. A.; Young, R. J.; Halsall, M. *Composites, Part A.* **2001**, *32*, 401.
(14) Meyer, J. C.; Paillet, M.; Roth, S. *Science* **2005**, *309*, 1539.
(15) Yang, X. P.; Wu, G.; Zhou, J.; Dong, J. M. *Phys. Rev. B* **2006**, *73*, 235403.
(16) Wu, G.; Zhou, J.; Dong, J. M. *Phys. Rev. B* **2005**, *72*, 115411.
(17) Cronin, S. B.; Swan, A. K.; Unlu, M. S.; Goldberg, B. B.; Dresselhaus, M. S.; Tinkham, M. *Phys. Rev. B* **2005**, *72*, 35425.
(18) Zhang, Y. Y.; Zhang, J.; Son, H. B.; Kong, J.; Liu, Z. F. *J. Am. Chem. Soc.* **2005**, *127*, 17156.
(19) Gao, B.; Duan, X. J.; Zhang, J.; Wu, T. J.; Son, H. B.; Kong, J.; Liu, Z. F. *Nano Lett.* **2007**, *7*, 750.
(20) Minot, E. D.; Yaish, Y.; Sazonova, V.; Park, J. Y.; Brink, M.; McEuen, P. L. *Phys. Rev. Lett.* **2003**, *90*, 156401.
(21) Souza, A. G.; Kobayashi, N.; Jiang, J.; Gruneis, A.; Saito, R.; Cronin, S. B.; Mendes, J.; Samsonidze, G. G.; Dresselhaus, G. G.; Dresselhaus, M. S. *Phys. Rev. Lett.* **2005**, *95*, 217403.
(22) Yang, L.; Han, J. *Phys. Rev. Lett.* **2000**, *85*, 154.
(23) Li, L. J.; Nicholas, R. J.; Deacon, R. S.; Shields, P. A. *Phys. Rev. Lett.* **2004**, *93*, 156104.
(24) Paillet, M.; Poncharal, P.; Zahab, A.; Sauvajol, J. L.; Meyer, J. C.; Roth, S. *Phys. Rev. Lett.* **2005**, *94*, 237401.

JP803434Y